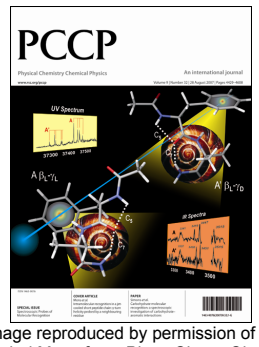

Image reproduced by permission of Dr Michel Mons from *Phys. Chem. Chem. Phys.*, 2007, **9**, 4491

This paper is published as part of a **PCCP** themed issue on

Spectroscopic probes of molecular recognition

Guest edited by Martin Suhm (Universität Göttingen)

Published in issue 32, 2007 of PCCP

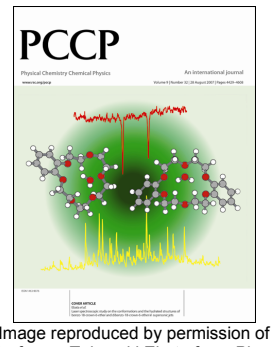

Image reproduced by permission of Professor Takayuki Ebata from *Phys. Chem. Chem. Phys.*, 2007, **9**, 4452

Other papers in this issue:

NMR studies of double proton transfer in hydrogen bonded cyclic *N*,*N*′-diarylformamidine dimers: conformational control, kinetic HH/HD/DD isotope effects and tunneling

Juan Miguel Lopez,† Ferdinand Männle,‡ Iwona Wawer,§ Gerd Buntkowsky¶ and Hans-Heinrich Limbach*

Received 26th March 2007, Accepted 14th May 2007
First published as an Advance Article on the web 25th June 2007
DOI: 10.1039/b704384h

Using dynamic NMR spectroscopy, the kinetics of the degenerate double proton transfer in cyclic dimers of polycrystalline ^{15}N,$^{15}N'$-di-(4-bromophenyl)-formamidine (DBrFA) have been studied including the kinetic HH/HD/DD isotope effects in a wide temperature range. This transfer is controlled by intermolecular interactions, which in turn are controlled by the molecular conformation and hence the molecular structure. At low temperatures, rate constants were determined by line shape analysis of ^{15}N NMR spectra obtained using cross-polarization (CP) and magic angle spinning (MAS). At higher temperatures, in the microsecond time scale, rate constants and kinetic isotope effects were obtained by a combination of longitudinal ^{15}N and ^{2}H relaxation measurements. ^{15}N CPMAS line shape analysis was also employed to study the non-degenerate double proton transfer of polycrystalline ^{15}N,$^{15}N'$-diphenyl-formamidine (DPFA). The kinetic results are in excellent agreement with the kinetics of DPFA and ^{15}N,$^{15}N'$-di-(4-fluorophenyl)-formamidine (DFFA) studied previously for solutions in tetrahydrofuran. Two large HH/HD and HD/DD isotope effects are observed in the whole temperature range which indicates a concerted double proton transfer mechanism in the domain of the reaction energy surface. The Arrhenius curves are non-linear indicating a tunneling mechanism. Arrhenius curve simulations were performed using the Bell–Limbach tunneling model. The role of the phenyl group conformation and hydrogen bond compression on the barrier of the proton transfer is discussed.

Introduction

In complex biological systems the function of biomolecules is often controlled by a molecular recognition process which in turn is controlled by molecular conformation and hence chemical constitution. In simple chemical systems such a series of events is less common. However, their advantage is that molecular details can be studied and understood. Symmetrically substituted *N*,*N*-diarylformamidines Ar–NH–CH=N–Ar (Fig. 1) and *N*,*N*-diaryltriazenes Ar–NH–N=N–Ar where Ar=X–C_6H_4 (Fig. 2) fall into this category. Here, the replacement of the central CH group in the *N*,*N*-diarylformamidines by a nitrogen atom leads to the class of *N*,*N*-diaryltriazenes. Both types of molecules behave in a very different way with respect to conformational isomerism, hydrogen bond association and proton exchange as has been shown in a series of liquid and solid state NMR studies from our laboratory. *N*,*N*-diarylformamidines—which are white—form an *S-cis* form and an *S-trans* form in tetrahydrofuran which are hydrogen bonded to the solvent as illustrated in Fig. 1.[1] At room temperature, the conformational isomerism is rapid within the NMR timescale, but slow exchange is achieved around 190 K. The spectra reveal that only the *S-trans* form can form cyclic dimers in which a double proton transfer takes place. The equilibrium constants of the monomer–dimer equilibrium and the concentration dependence of the rates of the proton tautomerism of the *S-trans* form could be elucidated, from which the intrinsic rate constants of the transfer in the cyclic dimers were obtained. In addition, kinetic HH/HD isotope effects were obtained for DPFA (X = H),[1] and the full kinetic HH/HD/DD isotope effects for DFFA (X = F) which indicated a concerted double proton transfer in a compressed dimer which takes place at low temperatures by tunneling.[2]

When we wanted to study the yellow *N*,*N*-diaryltriazenes as a reference we were surprised to find that these molecules were not able to form cyclic dimers and exchange their protons. However, in the presence of a base such as dimethylamine or trimethylamine an intramolecular H-transfer was observed, catalyzed by the base as illustrated in Fig. 2.[3] A detailed study

Institut für Chemie und Biochemie der Freien Universität Berlin, Takustrasse 3, D-14195 Berlin. E-mail: limbach@chemie.fu-berlin.de; Fax: +49 30 8385 5310; Tel: +49 30 8385 5375
† Present address: Leibniz-Institut für Molekulare Pharmakologie (FMP), D-13125 Berlin-Buch, Germany.
‡ Present address: SINTEF Materials and Chemistry, Forskningsveien 1, N-0314 Oslo, Norway.
§ Present address: Faculty of Pharmacy, Medical University of Warsaw, Ul. Banacha 1, Pl-02097 Warsaw, Poland.
¶ Present address: Institut für Physikalische Chemie, Friedrich Schiller Universität Jena, Helmholtzweg 4, D-07743 Jena, Germany.

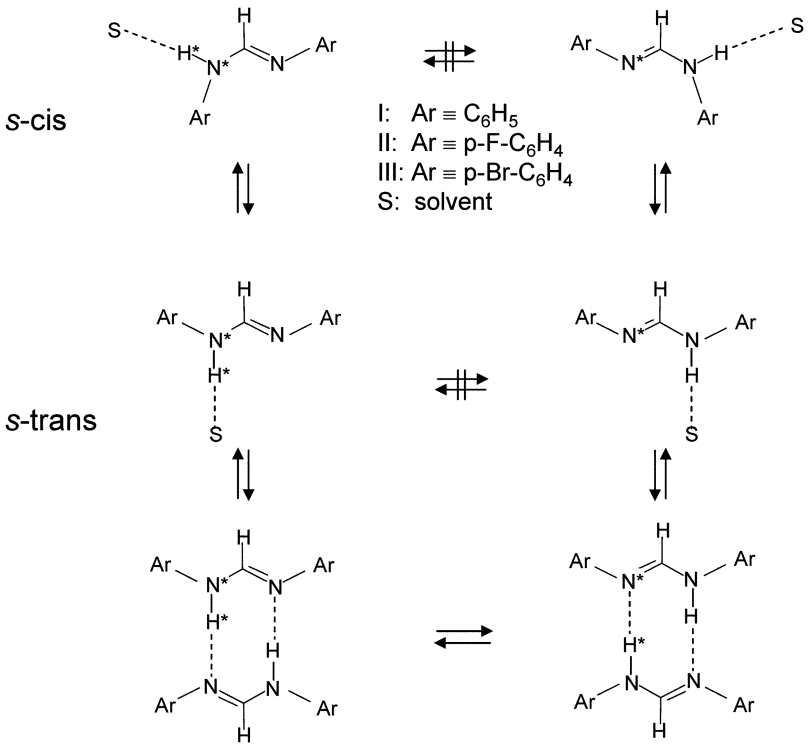

Fig. 1 *S-cis–S-trans* isomerism, cyclic hydrogen bond formation and double proton transfer of *N*,*N*-diarylformamidines dissolved in tetrahydrofuran according to ref. 1 and 2.

of kinetic H/D isotope effects and quantum-mechanical calculations indicated a transition state where H is transferred to the base.[4] We argued that the aryl rings play a more important role than anticipated in the beginning of our studies. Indeed, the aryl groups of *N*,*N*-diaryltriazenes in the solid state are coplanar with the triazene moieties which explains their yellow

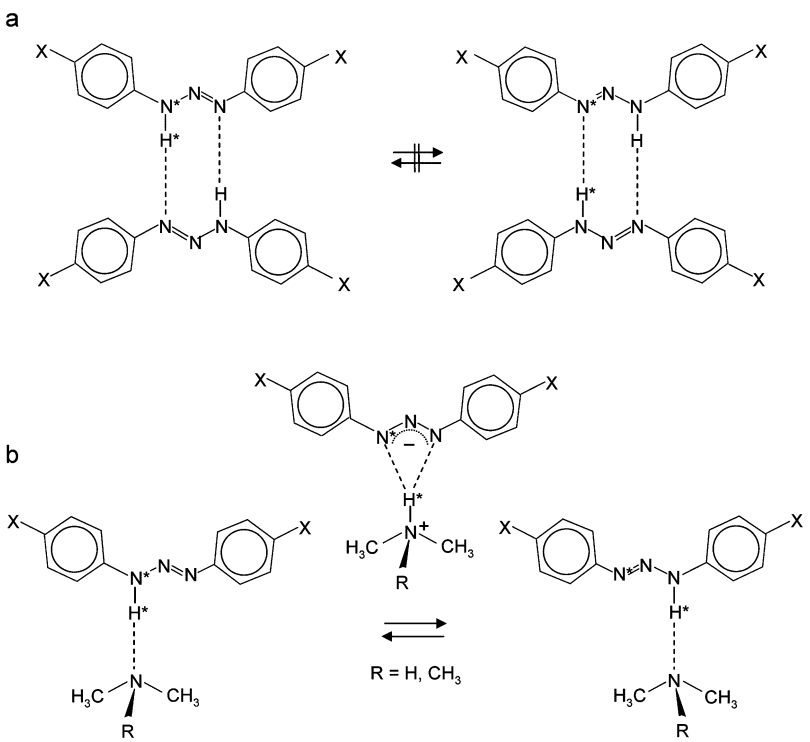

Fig. 2 Base catalyzed intramolecular proton transfer of *N*,*N*-diaryltriazenes according to ref. 3 and 4. Cyclic dimers are not formed because of steric repulsion between the aromatic CH protons.

color. Moreover, the molecules only form linear hydrogen bonded chains in which intermolecular steric interactions are minimized.[5] The fact that molecules cannot form cyclic hydrogen bonded dimers was discussed in terms of steric repulsion between the aryl rings as illustrated in Fig. 2. Thus, this repulsion should be absent in *N*,*N*-diarylamidines.

This is indeed the case as was shown by combined X-ray crystallography and high resolution solid state ^{15}N NMR spectroscopy using the conditions of cross polarization (CP) and magic angle spinning (MAS).[6] All *N*,*N*-diarylamidines studied formed cyclic dimers in the solid state as depicted for selected cases in Fig. 3, exhibiting N···N distances of about 3 Å. The aryl groups were found to be twisted from the formamidine plane with angles ϕ between 0 and 60°. The valence bond angles α increased when ϕ decreased, confirming the steric repulsion between the CH and the aromatic protons. On the other hand, this intramolecular interaction enables the formation of the cyclic dimers. Three different dimer types were found by NMR. The first type showed only a single tautomer in the solid state, from which it was concluded that the equilibrium constant of tautomerism $K = k_{12}/k_{21} \ll 1$, in contrast to the liquid state where $K = 1$. k_{12} and k_{21} are the forward and backward rate constants. An example is DFFA with X = F whose X-ray crystal structure is depicted in Fig. 3b. Here, the mobile protons are located on the amino nitrogens where the adjacent aryl group is essentially coplanar with the formamidine plane, *i.e.* exhibiting aryl torsional angles ϕ of 1.3 and 12.1°. By contrast, torsional angles ϕ of 44.3 and 58.7° were found for the imino nitrogen atoms. These results can be rationalized in terms of resonance effects of the nitrogen electron lone pairs with the adjacent aryl groups. By contrast, for DBrFA with X = Br a proton tautomerism was observed according to Fig. 3c which was degenerate within the NMR time scale.[6] Rate constants were obtained by line shape analysis and longitudinal relaxation measurements.[7] The crystal structure (Fig. 3d) gave an explanation: the torsional angles of the centro-symmetric dimer were very similar, *i.e.* 24.4 and 30.3°, leading to a similar basicity of all nitrogen atoms and hence to a degenerate double proton transfer process. Finally, for the third type of dimers non-degenerate proton transfer was observed with $K < 1$. An example is DPFA where X = H. Here, two very different torsional angles 59.3 and 9.3° were observed for one molecule but similar values, *i.e.* 37.7 and 30.7° for the other in the dimer, as depicted in Fig. 3e.

In previous studies we have studied the role of NHN hydrogen bond compression[8–12] on the mechanisms of degenerate or quasi-degenerate single and multiple proton transfers. It was shown that generally a reorganization energy is required in order to reach a state where the barrier of proton transfer is reduced by a decrease in the N···N distances. At about 2.5 Å, the NHN hydrogen bonds are so strong that the barrier for proton transfer vanishes. Moreover, hydrogen bond compression assists the switch from a potential stepwise to a concerted transfer.[2]

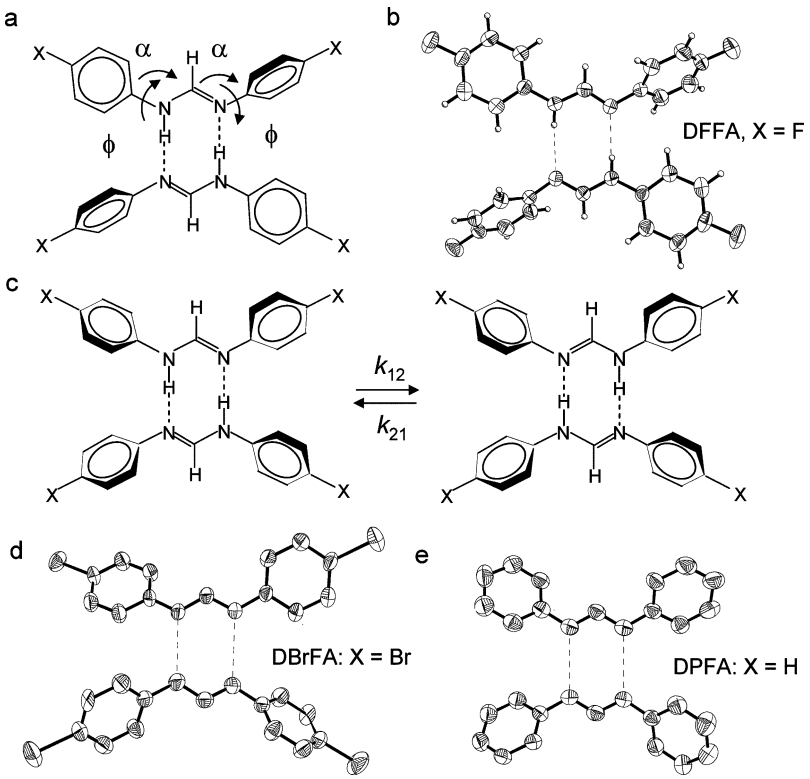

Fig. 3 Structure and tautomerism of cyclic dimers of crystalline *N*,*N*-diarylformamidines derived by ^{15}N solid state NMR and X-ray crystallography according to ref. 6. (a) Schematic structure of *N*,*N*-diarylformamidines dimers with localized NH protons. (b) Example: X-ray crystallographic structure of DFFA. (c) Schematic structure and tautomerism of cyclic *N*,*N*-diarylformamidines dimers exhibiting a solid state proton tautomerism. The degeneracy may be lifted by solid state interactions. (d) X-ray crystallographic structure of DBrFA exhibiting a degenerate tautomerism with $K = 1$. (e) X-ray crystallographic structure of DPFA exhibiting a non-degenerate tautomerism with $K < 1$.

Thus, we became interested again in the case of *N*,*N*-diarylamidines because the torsional motions of the aryl rings may not only control the degeneracy of the proton tautomerism but also the hydrogen bond compression. Therefore, we have undertaken a detailed dynamic solid state NMR study of the degenerate tautomerism of DBrFA where all torsional angles are similar. Using ^{15}N CPMAS NMR line shape analysis of partially deuterated DBrFA we have determined the full kinetic HH/HD/DD isotope effects below 150 K. At higher temperatures, these effects were determined using a combination of ^{15}N and ^{2}H longitudinal relaxation time measurements. For comparison, we also analyzed the ^{15}N CPMAS NMR line shapes of DPFA. Another goal of this study was to contribute to the theoretical understanding of the tautomerism in the amidines which are simple models for nucleic acid bases. To date, only very few *ab initio* calculations have been carried out on the unsubstituted compounds.[13]

This work is organized as follows: after a section describing the experimental aspects the results of the variable temperature ^{15}N CPMAS NMR line shape analyses and of the relaxation measurements performed on DPFA and DBrFA will be presented and analyzed. Finally, the non-linear Arrhenius curves obtained will be compared with those obtained previously for DPFA and DFFA using tetrahydrofuran as solvent, and the information obtained by this analysis discussed.

Experimental

^{15}N enriched DPFA and DBrFA were synthesized according to the method of Claisen[14] from triethylorthoformate and 95% enriched aniline-^{15}N (Chemotrade, Leipzig) and 4-bromoaniline-^{15}N. The latter was obtained using methods described for the unlabeled material.[15,16]

The ^{15}N CPMAS spectra were recorded at 9.12 MHz and 30.41 MHz using Bruker CXP 100 and MSL 300 NMR spectrometers equipped with a standard 7 mm and 5 mm Doty probeheads. We used a normal CP sequence, which minimizes ringing artifacts,[17] with 3–8 ms CP times, 6–10 μs ^{1}H-90° pulse width, 3–10 s recycle delay. For the measurement of the ^{15}N longitudinal relaxation times T_1 in connection with the CP scheme, a pulse sequence described by Torchia[18] was employed. Due to phase cycling of the first proton 90° pulse and of the receiver phase, the equilibrium magnetization is zero in this experiment, which is contrary to the most frequently applied inversion–recovery pulse sequence where equilibrium magnetization approaches maximum intensity. Between 500 and 2500 scans were accumulated on average, with a contact time for CP of between 1.5 and 5.0 ms, and a repetition time of 1–3 s. Low temperature measurements were carried out by passing nitrogen gas through a home built heat exchanger[19] immersed in liquid nitrogen, thus allowing temperatures as low as 90 K to be achieved, maintaining the spinning speeds between 2 and 2.5 kHz which were large enough for obtaining essentially rotational side band-free spectra. Chemical shifts were referenced to external solid $^{15}NH_4Cl$. For the line shape calculations a home-made computer program was used described previously,[20] based on the density matrix formalism proposed by Binsch *et al.*[21]

The measurements of the ^{2}H T_1 relaxation times for deuterated DBrFA were performed on a home-built 7 Tesla spectrometer operating at a Larmor frequency of 46.03 MHz, equipped with a home-built low temperature ^{2}H probe. The measurements were carried out employing a saturation recovery pulse sequence followed by a solid echo sequence and recording of the echo. The saturation part involved a string of 90° pulses (3.6 μs) with non-equal spacing to avoid any undesired echo formations. The two 90° pulses of the solid echo sequence were spaced by 35 μs. Finally, the echo was Fourier transformed, allowing the evaluation of T_1 of individual lines in the spectrum.

Results

Variable temperature ^{15}N NMR line shape analyses of DPFA and DBrFA

In Fig. 4a are depicted the superposed experimental and simulated variable temperature ^{15}N CPMAS NMR spectra of polycrystalline DPFA recorded at 9.12 MHz. At 100 K, two lines are observed at 180 ppm and at 84 ppm which are typical for the non-protonated and protonated nitrogen atoms. When temperature is increased, the lines broaden, shift towards each other and sharpen again as the rate constants of proton transfer increase. At room temperature the proton transfer is fast and a splitting of $\delta\nu = 22$ ppm is observed, which is strongly reduced compared to the intrinsic low-temperature splitting of $\Delta\nu \approx 96$ ppm. As has been shown many times,[22] this situation is typical for a non-degenerate proton tautomerism, where the equilibrium constant of the tautomerism is given in the fast exchange regime by

$$K_{12} = (1 - \delta\nu/\Delta\nu)/(1 + \delta\nu/\Delta\nu) = k_{12}/k_{21} = x_2/x_1 = \exp(\Delta S_{12}/R - \Delta H_{12}/RT). \quad (1)$$

ΔH_{12} and ΔS_{12} represent the reaction enthalpy and reaction entropy, R is the gas constant, k_{12} and k_{21} the forward and backward rate constants of the tautomerism and x_1 and x_2 the corresponding mole fractions. The spectra were simulated as described previously for other systems.[22] In order to simulate the spectra the values of K_{12} were first determined at high temperatures using eqn (1) and extrapolated to low temperatures,

$$K_{12} = 2.2 \times \exp(-307/T), \quad \Delta H_{12} = 3.05 \text{ kJ mol}^{-1}, \ \Delta S_{12} = 6.36 \text{ J K}^{-1} \text{ mol}^{-1}. \quad (2)$$

Then the exchange broadened spectra at lower temperatures were simulated by varying only k_{12}. The intrinsic chemical shifts were taken from the low-temperature spectra and the line width W_o in the absence of exchange from the spectra at 100 and 299 K. The rate and equilibrium constants obtained are included in Fig. 4a and Table 1.

Fig. 4b depicts the superposed experimental and calculated variable temperature ^{15}N CPMAS NMR spectra of polycrystalline DBrFA recorded at 9.12 MHz. At room temperature, only one singlet is observed at 134 ppm indicating that all nitrogen sites are equivalent within the margin of error. When

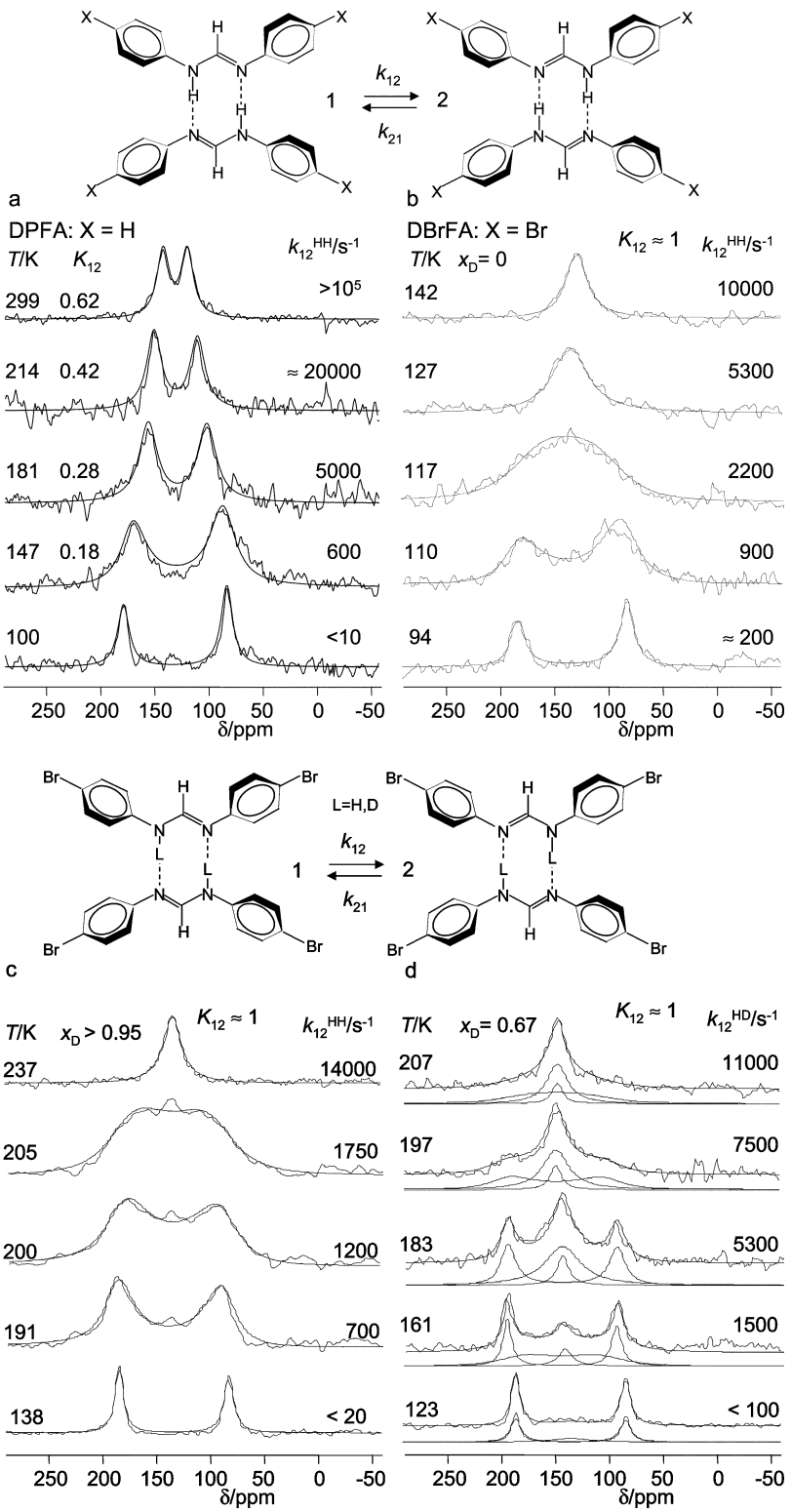

Fig. 4 Superposed experimental and calculated variable temperature ^{15}N CPMAS NMR spectra recorded at 9.12 MHz of polycrystalline $^{15}N,^{15}N$-diarylformamidines. (a) Polycrystalline DPFA-$^{15}N_2$ at a deuterium fraction of $x_D = 0$ in the mobile proton sites. (b)–(d) Polycrystalline DBrFA-$^{15}N_2$ at $x_D = 0$, $x_D > 0.95$ and $x_D = 0.67$. For further explanation see text.

the sample is cooled below 140 K the line broadens and eventually splits into two single lines at 83 and 185 ppm below the coalescence point of about 115 K. The high field line arises from the protonated and the low field line from the non-protonated nitrogen atoms; the small line distortions arise from different CP times of the two nitrogen sites.

As we observed only a single line in the fast exchange regime in the case of DBrFA the reduced splitting $\delta\nu$ must be smaller

Table 1 Equilibrium constants and forward and backward rate constants k_{12} and k_{21} obtained for the double proton transfer in solid DPFA by ^{15}N CPMAS line shape analysis

T/K	K_{12}	k_{12}^{HH}/s^{-1}	k_{21}^{HH}/s^{-1}
100	—	<10	<10
147	0.18	600	3300
181	0.28	5000	18 000
214	0.42	$\approx$20 000	$\approx$48 000
299	0.62	$>10^5$	$>10^5$

than the linewidth W_o in the absence of exchange. With $W_o \approx$ 4 ppm above 200 K, and $\Delta\nu \approx$ 102 ppm we estimate using eqn (1) values of K_{12} between 0.9 and 1.0. Hence, the proton tautomerism is degenerate within the margin of error, and, for the simulation of the line shapes, K_{12} was set to 1 in the whole temperature range. W_o was extrapolated from the line width in the slow and fast exchange regime and the rate constants $k = k_{12} = k_{21}$ assembled in Table 2 were obtained by simulation of the spectra as indicated in Fig. 4b.

Fig. 4c and d show the experimental and calculated ^{15}N CP MAS NMR spectra of DBrFA recorded at 9.12 MHz as a function of temperature at two different deuterium fractions

Table 2 Rate constants k_{12}^{HH}, k_{12}^{HD} and k_{12}^{DD} of double proton transfer in cyclic dimers of polycrystalline DBrFA obtained by ^{15}N CPMAS NMR line shape analysis at different deuteron fractions x_D

T/K	x_D	ν_o/MHz	k_{12}^{HH}/s^{-1}	k_{12}^{HD}/s^{-1}	k_{12}^{DD}/s^{-1}
110	0	9.12	900	—	—
117	0	9.12	2200	—	—
122	0	9.12	4200	—	—
127	0	9.12	5300	—	—
142	0	9.12	10 000	—	—
162	0.2	30.41	[a]	1200	—
163	0.2	30.41	[a]	1400	—
171	0.2	30.41	[a]	2500	—
176	0.2	30.41	[a]	3500	—
182	0.2	30.41	[a]	4700	—
188	0.2	30.41	[a]	6000	—
193	0.2	30.41	[a]	9100	—
200	0.2	30.41	[a]	11 000	—
204	0.2	30.41	[a]	12 000	—
169	0.8	30.41	[a]	3900	<50
176	0.8	30.41	[a]	4400	100[b]
189	0.8	30.41	[a]	8500	600[b]
197	0.8	30.41	[a]	13 000	950
202	0.8	30.41	[a]	14 500	1300
208	0.8	30.41	[a]	[a]	2200
161	0.67	9.12	[a]	1500	<50
168	0.67	9.12	[a]	2100	<50
173	0.67	9.12	[a]	3300	50[b]
183	0.67	9.12	[a]	5300	200[b]
197	0.67	9.12	[a]	7500	1100
207	0.67	9.12	[a]	11 000	2200
191	0.95	9.12	[a]	[a]	700
200	0.95	9.12	[a]	[a]	1200
205	0.95	9.12	[a]	[a]	1750
208	0.95	9.12	[a]	[a]	2200
211	0.95	30.41	[a]	[a]	3000
214	0.95	30.41	[a]	[a]	3300
217	0.95	30.41	[a]	[a]	4200
222	0.95	30.41	[a]	[a]	5600
237	0.95	30.41	[a]	[a]	14 000

[a] Values larger than 20 000 s^{-1} without influence on the line widths. [b] Extrapolated values.

x_D of the mobile proton sites. For a statistical distribution, the mole fractions of the isotopologs is given by

$$x_{HH} = (1 - x_D)^2, x_{HD} = 2(1 - x_D)x_D, x_{DD} = x_D^2 \qquad (3)$$

At a deuterium fraction of $x_D > 0.95$, the mole fractions of the isotopologs are given by $x_{DD} > 0.9$ and $x_{HD} < 0.1$, $x_{HH} <$ 0.0025. Thus, in good approximation, the line shape is determined only by k_{12}^{DD}. The results of the simulations are assembled in Table 2.

In order to obtain the rate constants k_{12}^{HD} we measured a sample with a deuterium fraction of $x_D \approx 0.67$, where we expect that $x_{HH} = 0.11$, $x_{HD} = 0.445$, $x_{DD} = 0.445$. As the values of k_{12}^{HH} and of k_{12}^{DD} could be extrapolated from the measurements at $x_D = 0$ and 0.95, we only needed to adjust the values of k_{12}^{HD} and the line intensities of the different isotopologs which can be different from the mole fractions because of intensity distortions arising from CP. Therefore, the line intensities are not discussed further. However, as illustrated in Fig. 4d, the total line shapes can be described well in terms of the sums of the line shape contributions of the different isotopologs. The rate constants k_{12}^{HD} obtained in this way are included in Table 2.

Additional experiments were recorded at 30.41 MHz at deuterium fractions of 0.8 and 0.2. Some typical results are depicted in Fig. 5. The line shapes were again decomposed into the contributions of the three isotopologs, and again only their line intensities and the values of k_{12}^{HD} needed to be adapted. Spinning speeds were so high (5–9 kHz) that rotational side bands could mostly be avoided. Because of sample heating in the case of the high speed probe, a small quantity of ^{15}N labeled tetramethyltetraaza[14]annulene (TTAA) was added to the rotors in a separate capsule in order to obtain the sample temperatures from the four temperature-dependent ^{15}N chemical shifts of this compound[23] marked by asterisks in Fig. 5. Thus, by line shape analysis not only k_{12}^{HD} but also the temperature was obtained. The temperature error is, however, a few degrees. Because of the higher resolution at 30.41 MHz we noticed that both the two amino as well as the two imino nitrogen atoms of the cyclic dimers of DBrFA exhibit slightly different chemical shifts as expected from the crystal structure. These splittings were taken into account in the line shape simulations.

We noticed that the rate constants k_{12}^{HD} obtained at $x_D =$ 0.2 are slightly smaller than those obtained at $x_D = 0.8$. In view of the margin of error of the temperature we do not discuss this difference further.

Variable temperature ^{15}N NMR longitudinal relaxation times and rates of HH-transfer in DBrFA

In order to obtain rate constants of the double proton transfer at higher temperatures, longitudinal ^{15}N relaxation times were measured for non-deuterated DBrFA at 9.12 MHz. This Larmor frequency is small enough so that only a ^{1}H–^{15}N dipolar relaxation mechanism needs to be considered, *i.e.* that relaxation contributions from the modulation of the chemical shielding anisotropy by the proton motion can be neglected.[24] The magnetization decays were found to be exponential in the whole temperature range. The T_1 values obtained by non-

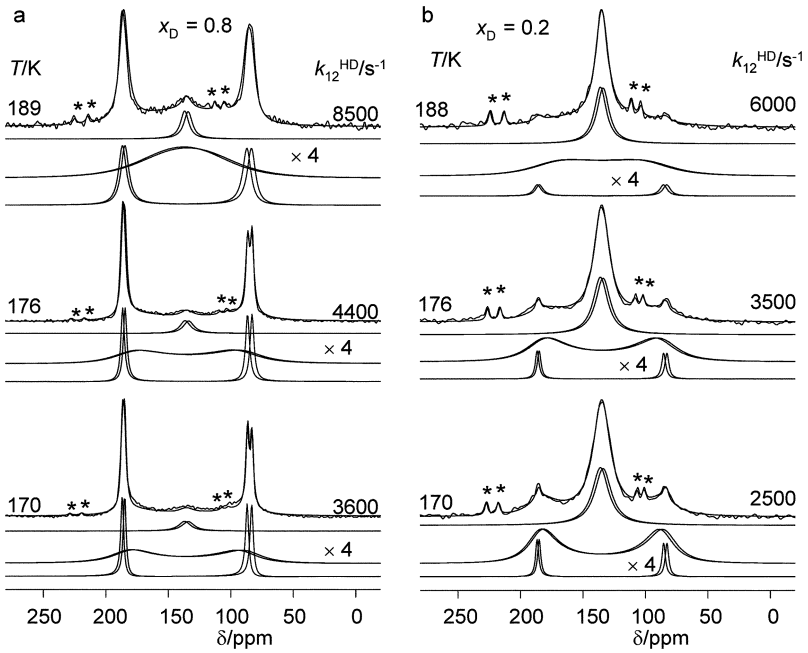

Fig. 5 Superposed experimental and calculated variable temperature ^{15}N CPMAS NMR spectra recorded at 30.41 MHz of polycrystalline DBrFA-$^{15}N_2$ at a deuterium fraction of $x_D = 0.8$ (a) and $x_D = 0.2$ (b) in the mobile proton sites. For further explanation see text.

linear least squares fitting are assembled in Table 3 and plotted in Fig. 6 in a logarithmic scale as a function of the inverse temperature. They exhibit the typical behavior of a thermally activated process. The observation of the minimum around 330 K allowed us to verify that the modulation of the heteronuclear dipolar ^{1}H–^{15}N interaction together with the fast proton motion is responsible for the longitudinal relaxation observed, as described in the following.

As shown previously,[24] under MAS conditions, in the presence of a two-state tautomeric equilibrium, the ^{15}N T_1 values are given in very good approximation by the isotropic average

$$\frac{1}{T_{1S}} = \frac{1}{30}\gamma_I^2\gamma_S^2\hbar^2(\mu_0/4\pi)^2 S(S+1)R_{SI}\frac{4K_{12}}{(1+K_{12})^2} \times \left[\frac{\tau_c}{1+(\omega_I-\omega_S)^2\tau_C^2} + \frac{3\tau_c}{1+\omega_S^2\tau_C^2} + \frac{6\tau_c}{1+(\omega_I+\omega_S)^2\tau_C^2}\right]. \quad (4)$$

where μ_0 is the permeability of the vacuum, γ_I and γ_S the gyromagnetic ratios of spin I of hydrogen and S of nitrogen, ω_I and ω_S the corresponding Larmor frequencies, h Planck's constant. The inverse correlation time of the tautomerism is given by

$$\frac{1}{\tau_c} = k_{12} + k_{21} \quad (5)$$

Finally, the dipolar ^{1}H–^{15}N interaction gives rise to the geometric factor

$$R_{SI} = R_{NH} = r_{NH}^{-6} + r_{H\cdots H}^{-6} + r_{NH}^{-3}r_{H\cdots N}^{-3}(1-3\cos^2\alpha) \quad (6)$$

Table 3 Rate constants k_{12}^{HH} of double proton transfer in cyclic dimers of polycrystalline DBrFA obtained by ^{15}N CPMAS ^{15}N-T_1 relaxation times

T/K	^{15}N T_1/s	k_{12}^{HH}/s^{-1}	T/K	^{15}N T_1/s	k_{12}^{HH}/s^{-1}
240	3.85	1.75×10^6	296	0.56	1.57×10^7
240	2.89	2.35×10^6	305	0.52	1.75×10^7
250	2.72	2.50×10^6	321	0.49	2.14×10^7
251	2.78	2.44×10^6	326	0.47	3.73×10^7
252	3.01	2.25×10^6	336	0.48	4.15×10^7
260	1.43	4.84×10^6	356	0.59	6.65×10^7
264	1.35	5.15×10^6	370	0.62	7.31×10^7
272	1.04	6.88×10^6			

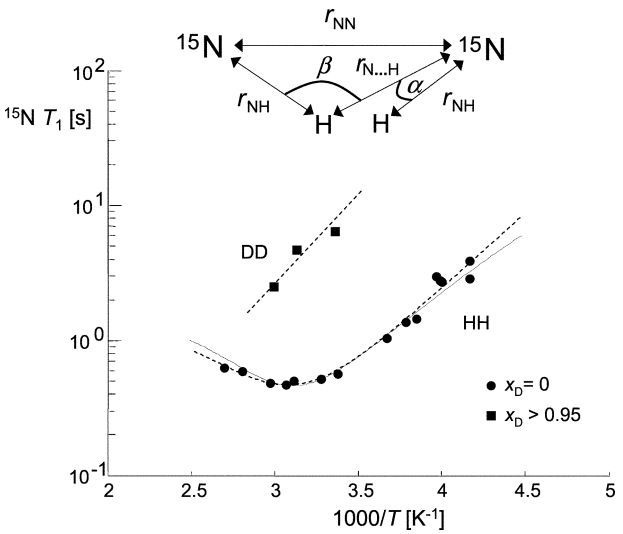

Fig. 6 Longitudinal ^{15}N relaxation times T_1 of polycrystalline DBrFA-$^{15}N_2$ measured at 9.12 MHz under MAS conditions at different deuterium fraction x_D in the mobile proton sites. The HH data were taken from ref. 7. The values of ^{15}N T_1 at 9.12 MHz and $x_D > 0.95$ were 8.7 s, 5.5 s, 2.6 *s* at 298 K, 320 K, 334 K. For further explanation see text.

where r_{NH} represents the short N–H bond length and $r_{H\cdots N}$ the long hydrogen bond length, and α represents the jump angle as depicted in Fig. 6, whereas the hydrogen bond angle β does not directly enter eqn (6).

In a first stage the data were fitted to eqn (4) assuming an Arrhenius law of the degenerate double proton transfer from which an energy of activation of 21.3 kJ mol^{-1} and an effective pre-exponential factor $\log(A/s^{-1}) = 10.9$ was obtained,[7] as well as a value of $R_{NH} = 0.535$ Å^{-6}. The calculated line corresponds to the lower dashed line in Fig. 6. In a second stage, the value of R_{NH} was used in order to convert the ^{15}N T_1 values into the rate constants k_{12} using eqn (4). For this conversion a computer program was written which varied k_{12} until eqn (4) was fulfilled. The rate constants obtained in this way are included in Table 3. Finally, in the last stage, the ^{15}N T_1 values were recalculated using the non-linear Arrhenius curve of the HH transfer depicted in Fig. 10, calculated using the Bell–Limbach tunnel model as discussed below, giving rise to the solid line in Fig. 6.

In order to obtain rate constants of the HD and the DD transfer using this method we performed some ^{15}N T_1 measurements at higher deuterium fractions. Some data obtained at $x_D > 0.95$ are included in Fig. 6. However, because of the much smaller gyromagnetic ratio of deuteron and because of the large kinetic isotope effects the dipolar contribution to the longitudinal ^{15}N relaxation values is drastically reduced. This leads to substantially larger values of T_1 as illustrated in Fig. 6. Under these conditions, the contribution to the longitudinal relaxation arising from the modulation of the chemical shift anisotropy by the double proton transfer can no longer be neglected.[24] Therefore, we did not try to obtain kinetic information from the longitudinal relaxation measurements performed after partial H/D substitution.

Variable temperature ^{2}H NMR longitudinal relaxation times and rates of HD/DD-transfer in DBrFA

In order to obtain rate constants of the HD and the DD transfer we performed ^{2}H NMR relaxation measurements. In a first stage, 46.03 MHz ^{2}H NMR spectra of DBrFA were recorded at deuterium fractions in the mobile proton sites of $x_D \approx 0.1$ and >0.95 recorded under MAS conditions as shown in Fig. 7. The spinning speed used was 6 kHz which allowed us to considerably increase the signal to noise ratio as compared to measurements of a static sample, *i.e.* to a considerable reduction in the acquisition time, keeping the typical double Pake ^{2}H line shape. Assuming a statistical distribution of isotopologs, the signal intensity of the DD species is given by x_D and of the HD species by $1 - x_D$. In other words, at $x_D > 0.95$ the signal contribution of the HD species can be neglected. At $x_D \approx 0.1$, the signal stems to about 90% from the HD and to about 10% from the DD species.

By the line shape analysis depicted in Fig. 7 a quadrupolar coupling constant of $q_{cc} = 4/3q_{zz} = 160$ kHz and an asymmetric factor $\eta = (q_{xx}–q_{yy})/q_{zz} = 0.18$ were obtained for both samples, indicating that substitution of the second H by D in a cyclic dimer does not affect the components q_{xx}, q_{yy}, q_{zz} of the quadrupole coupling tensor within the margin of error. We note that the values obtained do not refer to the intrinsic

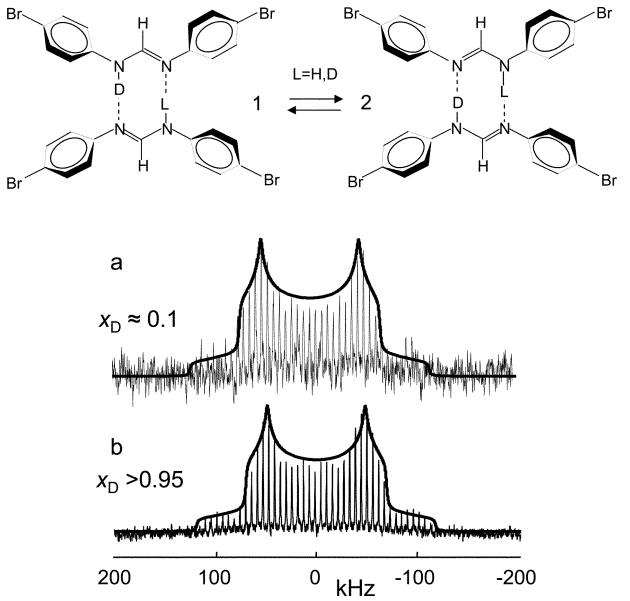

Fig. 7 Superposed experimental and calculated ^{2}H NMR spectra of DBrFA-$^{15}N_2$ measured at 46.03 MHz and a temperature of 298 K under MAS conditions. Spinning speed 6 kHz. Quadrupolar echo pulse sequence used. Variable delay VD = 12 s. (a) $x_D = 0.1$. (b) $x_D > 0.95$. For further explanation see text.

quadrupole coupling tensor but to a tensor averaged by fast deuteron transfer. This regime is reached as the motion of the deuterons is highly anisotropic and as the rate constants of the HD and DD transfer are of the order of 10^6 Hz as shown later.

In a second stage, longitudinal ^{2}H relaxation times T_1 were measured using a conventional saturation recovery experiment as depicted in Fig. 8a. An example is depicted in Fig. 8a. The T_1 values were obtained by fitting the signal intensities to

$$\begin{aligned} \text{Int} = &\text{Int}_\infty[x_D(1 - \exp(-t/T_1^{DD})) + (1 - x_D) \\ &\times (1 - \exp(-t/T_1^{HD}))] \end{aligned} \quad (7)$$

where T_1^{DD} and T_1^{HD} represent the ^{2}H longitudinal relaxation times of the DD and the HD isotopologs. An illustration is given in Fig. 8b. At $x_D > 0.95$ the signal decay is entirely governed by the DD jumps and the contribution of the HD isotopolog to eqn (7) can be neglected. The decay at $x_D \approx 0.1$ is much faster because of the faster HD jumps. In order to obtain T_1^{HD}, in the data analysis the second term eqn (7) was taken into account, but the values of T_1^{DD} were taken from those obtained at $x_D > 0.95$. All relaxation times measured are assembled in Table 4 and are plotted as a function of the inverse temperature in Fig. 9.

In order to obtain rate constants of the HD and the DD jumps of DBrFA we proceeded as follows. It has been shown that the longitudinal relaxation times of a deuteron with spin $I = 1$, jumping between two states can be expressed as:[25]

$$\frac{1}{T_{1I}} = \frac{3\pi^2}{10} C \frac{K_{12}}{(K_{12}+1)^2}\left[\frac{\tau_c}{1+\omega_I^2\tau_c^2} + \frac{4\tau_c}{1+4\omega_I^2\tau_c^2}\right] \quad (8)$$

For axially symmetric quadrupole coupling constant tensors the prefactor C can be expressed as[25]

$$C = q_{cc}(1)^2 + q_{cc}(2)^2 - q_{cc}(1)q_{cc}(2)(3\cos^2\theta - 1) \quad (9)$$

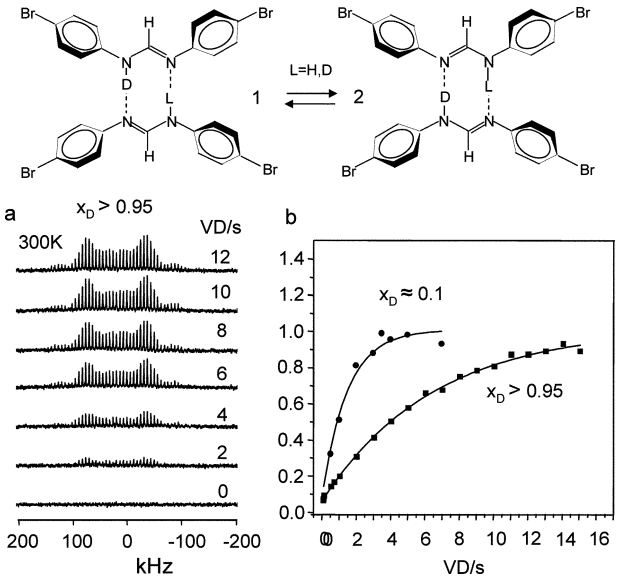

Fig. 8 Longitudinal ^{2}H relaxation time measurements of DBrFA-$^{15}N_2$ measured under MAS conditions at 46.03 MHz at $x_D \approx 0.1$ and $x_D > 0.95$. (a) Progressive saturation experiment at $x_D > 0.95$, (b) Signal intensities as a function of VD. For further explanation see text.

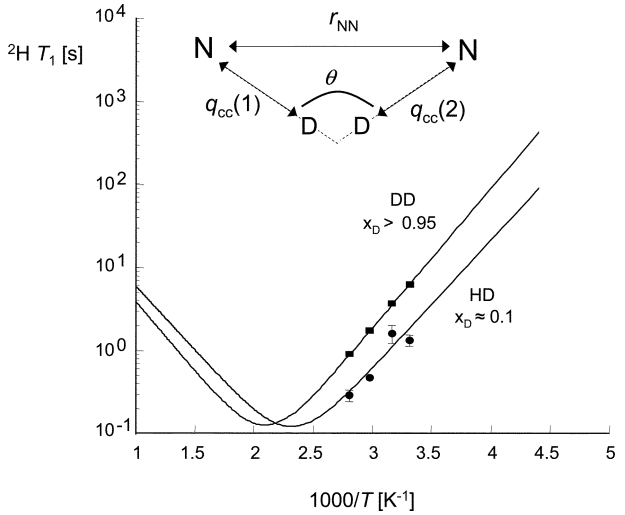

Fig. 9 Longitudinal ^{2}H relaxation times T_1 of DBrFA-$^{15}N_2$ measured under MAS conditions at 46.03 MHz at $x_D \approx 0.1$ and $x_D > 0.95$ as a function of the inverse temperature. For further explanation see text.

where $q_{cc}(1) = q_{cc}(2)$ represent the intrinsic quadrupole coupling constants in both tautomeric forms and θ the jump angle between the main axes of the quadrupolar coupling tensor in the two states as defined in Fig. 9. However, eqn (9) is an approximation and generally the factor C has to be determined experimentally from the value of T_1 in the minimum. Unfortunately, in the case of DBrFA, the latter could not be reached because the melting point is around 440 K.[15b]

Therefore, we proceeded as follows. Firstly, we assumed that the values of C are the same for the HD and the DD isotopologs, in agreement with the finding that the ^{2}H NMR line shapes of the deuterons in both species are the same. Secondly, we noticed that in the analysis of the Arrhenius curves of the tautomerism of DBrFA described in the next section the high temperature limit is reached for the HD and the DD transfers, where exponential Arrhenius curves are observed governed by the true pre-exponential factors A. The latter are—within the margin of error—isotope insensitive.[10] From the HH data this value was determined to be $10^{12.4}$ s^{-1}. Using this value and eqn (8), we could adapt the solid lines in Fig. 9 to the experimental values by only adapting the corresponding energies of activation. We obtained values of 30.1 kJ mol^{-1} for the HD and of 33.1 kJ mol^{-1} for the DD process from which we predict T_1 minima around 475 K for the DD and of 425 K for the HD isotopolog. Thus, we could generate the rate constants of the HD and DD reactions in the high-temperature limit listed in Table 4 as well as the value of $C = 9.84 \times 10^8$ s^{-2}. Using eqn (9) *i.e.* a quadrupole coupling constant of $q_{cc}(1) = q_{cc}(2) = 160$ kHz we predict a jump angle of $\theta = 173°$. This value is in good agreement with a hydrogen bond angle $\beta = 5°$ defined in Fig. 6 and indicates the presence of fairly linear hydrogen bonds. This feature is also the reason why the ^{2}H quadrupole relaxation mechanism is not much more effective as compared to the dipolar ^{15}N–^{1}H relaxation mechanism: the latter is operative even in the case of linear hydrogen bonds whereas the former vanishes at $\theta = 180°$ according to eqn (9).

As the Arrhenius parameters were now known for the HD and the DD reaction, we could convert the experimental T_1 values into the corresponding rate constants, listed in Table 4.

Table 4 Rate constants k_{12}^{HD} and k_{12}^{DD} of double hydron transfer in cyclic dimers of polycrystalline DBrFA obtained from ^{2}H T_1 relaxation times measured for static samples

T/K	T_1^{HD}/s	k_{12}^{HD}/s^{-1}	T_1^{DD}/s	k_{12}^{DD}/s^{-1}
301	1.4	5.5×10^6	6.52	7.1×10^5
316	1.7	4.4×10^6	3.34	1.3×10^6
336	0.5	1.2×10^7	1.82	2.8×10^6
356	0.31	2.6×10^7	0.94	5.5×10^6

Discussion

Using a combination of various methods of dynamic solid state NMR we have measured the kinetic HH/HD/DD isotope effects of the degenerate double proton transfer in cyclic dimers of polycrystalline ^{15}N,$^{15}N'$-di-(4-bromophenyl)-formamidine (DBrFA) in a wide temperature range. Some rate constants were also obtained for polycrystalline ^{15}N,$^{15}N'$-di-(phenyl)-formamidine (DPFA) where the gas phase degeneracy of the HH transfer is lifted by intermolecular interactions. In this section, we will firstly describe the parameters used to simulate the Arrhenius curves of double proton transfers in the presence of tunneling. Then we discuss the parameters obtained by these simulations and discuss them in comparison with some other known related double proton transfer reactions.

Arrhenius curve simulation parameters of degenerate double proton transfer

Tunneling model. The Arrhenius curves of the double proton transfers discussed below were calculated using a full Bell

tunneling model modified by Limbach *et al.* (''Bell–Limbach-model'').[10–12] In the framework of this model, the Arrhenius curve of each isotopic reaction LL = HH, HD, DD depends on five parameters, A, E_m, E_d^{LL}, Δm, $2a^{LL}$. The following parameters are experimental quantities: (i) the pre-exponential factor A determines the intercept of the Arrhenius curve at high temperatures; (ii) E_m corresponds to the slope of the Arrhenius curve in the strong tunneling regime at low temperatures and (iii) the slope at high temperatures by $E_m + E_d^{LL}$ where E_d^{LL} is the barrier height in the tunneling configuration. In the absence of pre-equilibria, A is in the usual range for solid state proton transfers,[11,12] which is of the order of $10^{12.6}$ s^{-1}. Traditionally, E_m has been neglected resulting in temperature independent rate constants of tunneling at low temperatures. However, it has been observed in various hydrogen transfer reactions in organic molecules[26,27] and in enzyme reactions.[28,29] It corresponds to any atomic and molecular displacements preceding the tunnel process. Therefore, it is isotope insensitive. Various sources contribute to E_m as has been discussed before.[2,10–12,26,27] For example, in a stepwise double proton transfer it contains a term necessary to reach the energy of the intermediate state below which tunneling cannot occur. For liquid solution solvent reorientation or non-recognized pre-equilibria can play a role.[11,12] Furthermore, E_m contains a term necessary for the reorganization of the molecular skeleton or the compression of the hydrogen bond. This contribution is equivalent to the ''work term'' in Marcus theory of electron and proton transfer.[30]

The hydron tunneling masses correspond to the sum of the masses of the particles which tunnel, *i.e.* 1 and 2 for H and D in a single hydron transfer and to 2, 3 and 4 in a HH/HD/DD transfer and are not varied. However, there might be small displacements of heavy atoms during the tunnel process which enhances the tunneling mass, taken into account by the parameter Δm. Finally, $2a^{LL}$ corresponds to the width of the barrier assumed to be parabolic.

Only in special cases is it possible to obtain all five parameters from the Arrhenius curve of a single isotopic reaction. The situation is, however, different in the case of a set of three Arrhenius curves for the HH, HD and DD reaction. The Arrhenius curves of the HD and the DD reactions require each only a single additional parameter, *i.e.* the modified barrier heights E_d^{HD} and E_d^{DD}. This is because the isotopic sensitive barrier widths depend on the heights, *i.e.*[11]

$$2a^{HD} = 2a^{HH}\sqrt{\frac{E_d^{HD}}{E_d^{HH}}},\ 2a^{DD} = 2a^{HH}\sqrt{\frac{E_d^{DD}}{E_d^{HH}}} \qquad (10)$$

In the presence of a concerted double proton transfer it has been shown that often the barrier increase induced by substitution of the first H by D is similar to the substitution of the second H by D, *i.e.* that[11]

$$E_d^{HD} = E_d^{HH} + \Delta\varepsilon,\ E_d^{DD} = E_d^{HD} + \Delta\varepsilon \qquad (11)$$

This assumption leads at high temperatures where the over-barrier dominates to the rule of the geometric mean for the isotopic rate constants

$$\frac{k^{HH}}{k^{HD}} = \frac{k^{HD}}{k^{DD}},\ k^{HD} = \sqrt{k^{HH}k^{DD}}. \qquad (12)$$

However, this rule is also fulfilled in good approximation at low temperatures as barrier height, width, and tunneling mass of the HD reaction correspond practically to the arithmetic mean of the HH and the DD reaction. Only at intermediate temperatures, where the tunneling contributions to the DD and the HD reactions are smaller than to the HH reaction, the first isotope effect is larger than the second, as has been observed several times[11]

$$\frac{k^{HH}}{k^{HD}} > \frac{k^{HD}}{k^{DD}} \qquad (13)$$

By contrast, for a stepwise degenerate double proton transfer it has been shown[11] that

$$k^{HD}/k^{DD} = \frac{2}{1 + k^{DD}/k^{HH}} \cong 2 \ \text{ for } \ k^{HH}/k^{DD} \gg 1. \qquad (14)$$

Thus, only the six parameters A, E_m, Δm, $E_d^{HH} = E_d$, $2a^{LL} = 2a$ and $\Delta\varepsilon$ are necessary to simulate the Arrhenius curves of the three isotopic reactions. For these simulations a non-linear least squares fitting routine was used, where each parameter could be varied automatically or manually.

We are aware that this model is not perfect. It is only a preliminary approach to interpreting experimental Arrhenius curves until a fully quantum-mechanical description is available that will provide better quantitative support for the qualitative interpretation of the Bell–Limbach model. Note that in the case of the proton exchange between acetic acid and methanol, the kinetic data were published in 1984,[10a] and a quantum-mechanical model using an instanton approach was published by Smedarchina *et al.* only in 2001.[31]

Arrhenius curve simulations. In Fig. 10 we have plotted the Arrhenius diagram of the HH, HD and DD transfer in cyclic dimers of polycrystalline DBrFA. For comparison, Fig. 11 depicts the corresponding graph for DFFA dissolved in

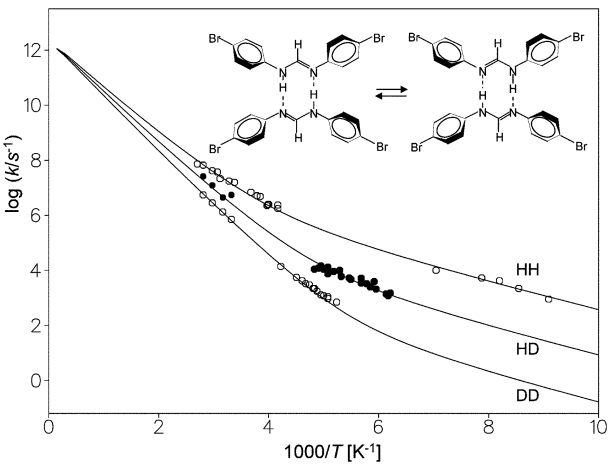

Fig. 10 Arrhenius diagram of the degenerate solid state HH, HD and DD tautomerism of cyclic dimers of DBrFA. The solid lines were calculated using the Bell–Limbach tunneling model. For further explanation see text.

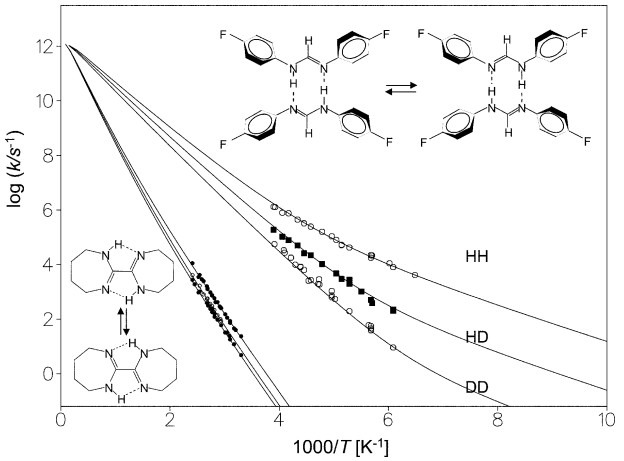

Fig. 11 Arrhenius diagram of the degenerate HH, HD and DD tautomerism inside cyclic dimers of DFFA-$^{15}N_2$ dissolved in tetrahydrofuran-d_8. Adapted from ref. 2*b*. For further explanation see text.

tetrahydrofuran[2] and Fig. 12 the data obtained for DPFA in the polycrystalline state and dissolved in tetrahydrofuran.[1] The latter are assembled in Table 5. Moreover, we have included in Fig. 11 the Arrhenius curve of the intramolecular double proton transfer in the seven-membered bicyclic oxalamidine OA7 (2,2′-bis(4,5,6,7-tetrahydro)-1,3-diazepine, Fig. 13a) dissolved in methylcyclohexane.[32]

The Arrhenius curve simulation parameters were derived as follows. Firstly, the Arrhenius curves were simulated without automatic parameter fit. As anticipated, we found that a common value of $10^{12.4}$ s^{-1} for the pre-exponential factors A of all isotopic reactions could well describe the experimental data. For DBrFA, the isotope insensitive value of E_m could be determined without assumptions from the Arrhenius curve of the HH reaction in Fig. 10. Then, E_d^{HH} and $\Delta\varepsilon$ was determined from the slopes of the Arrhenius curves at high temperatures. Finally, Δm and $2a$ were determined from the effective pre-exponential factors of the HH and the HD reactions in the

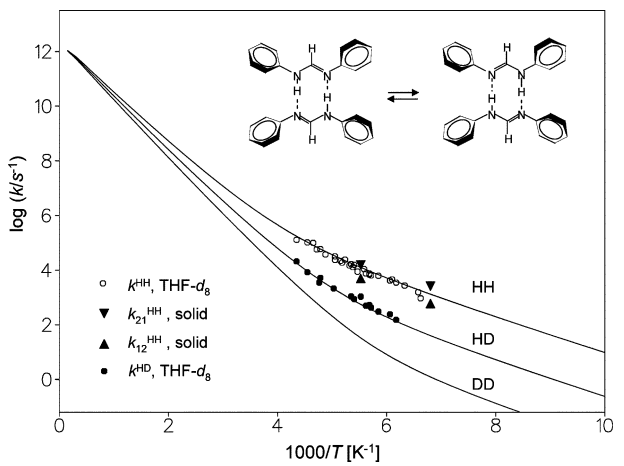

Fig. 12 Arrhenius diagram of the degenerate HH and HD tautomerism inside cyclic dimers of DPFA dissolved in tetrahydrofuran-d_8. Black triangles: Backward rate constants in polycrystalline DPFA. Adapted from ref. 1. For further explanation see text.

Table 5 Rate constants $k_{12} = k_{21}$ obtained for the double proton transfer in cyclic dimers of DPFA dissolved in THF-d_8 according to ref. 1

T/K	k_{12}^{HH}/s^{-1}	k_{12}^{HD}/s^{-1}	T/K	k_{12}^{HH}/s^{-1}	k_{12}^{HD}/s^{-1}
151	940		187	16 600	1100
152	1570		188	14 800	
158	2750		191	24 300	
162	3540	152	193	18 900	—
164	4620	—	194	21 900	
165	4170	243	198	32 200	
171	6240	305	198	23 800	
175	6450	428	199	32 000[a]	2150
176	6900	536	205	37 700	—
176	7570	—	209	59 000	5250
178	7600	500	210	—	3548
179	11 000	—	212	57 300	—
181	—	1080	215	99 600	—
183	8870	—	220	103600	8430
185	15 600	870	230	128900	20 893
186	12 900				

[a] Extrapolated values.

low-temperature tunneling regime. The corresponding parameters for the other reactions in Table 6 were obtained previously using a similar strategy.

In Table 6 we have included for comparison the parameters obtained previously[11] for the related double proton transfers in solid benzoic acid dimers,[33,34] derived from the data of Horsewill *et al.*,[34] and in 3,5-diphenyl-4-Br-pyrazole (DPBrP) (Fig. 13b and c).[9]

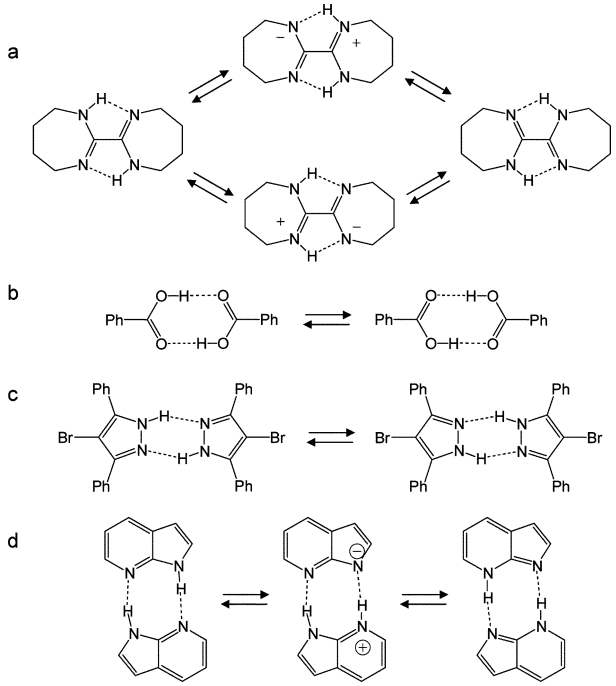

Fig. 13 (a) Tautomerism of 2,2′-bis(4,5,6,7-tetrahydro)-1,3-diazepine (OA7) in organic solvents.[32] (b) Solid state tautomerism of benzoic acid dimers.[33,34] (c) Solid state tautomerism of 3,5-diphenyl-4-Br-pyrazole (DPBrP).[9] (d) Photoinduced tautomerism of 7-azaindole dimers.[36,37]

Table 6 Geometric data, kinetic data and Arrhenius curve simulation parameters of various degenerate double proton transfers in cyclic hydrogen bonded dimers

	Geometric and kinetic data			Arrhenius curve simulation parameters					
System	H-bond geometry	k^{HH}(298 K)/ s^{-1}	*KIE*(298 K)	E_m/ kJ mol^{-1}	log (A/s^{-1})	E_d/ kJ mol^{-1}	Δm/ a.m.u.	$2a^H$ /Å	$\Delta\varepsilon$/ kJ mol^{-1}
DFFA in THF-d_8 ref. 2	—	9.4×10^6	HH/HD 4.7 HD/DD 4.0 HH/DD 19	11.7 (5.4)[a]	12.4 (12.2)[a]	21.7 (26.4)[a]	0.5 (1.05)[a]	0.48 (0.55)[a]	HH/HD 3.0 HD/DD 3.0
DPFA in THF-d_8 ref. 1	—	3.4×10^6	HH/HD 4.4 HD/DD 3.5 HH/DD 15	11.7	12.4	25.1	0.5	0.46	HH/HD 2.5 HD/DD 2.5
DBrFA this work	r_{NN} = 2.963 Å[6]	1.3×10^7	HH/HD 5.6 HD/DD 4.1 HH/DD 23	9.2	12.4	24.7	0.5	0.44	HH/HD 2.9 HD/DD 2.9
Oxalamidine OA7 in methylcyclo-hexane ref. 32*c*	r_{NN} = 2.8/3.0 Å[c]	14	HH/HD 3.1 HD/DD 1.5	52.7	12.6	27.2	1.5	0.2	H/D 2.9
$(PhCOOH)_2$ crystal ref. 34	r_{OO} = 2.606 Å q_1 = 0.3115 Å[b] q_2 = 2.609 Å[b]	9×10^{10}	HH/HD 2.4 HD/DD 6	HH 0.84 HD 0.84 DD 1.06	11.6	5.4	1.8	HH 0.48 HD 0.52 DD 0.44	HH/HD 2.1 HD/DD 4.6
3,5-diphenyl-4-Br pyrazol crystal ref. 9	r_{NN} = 2.84 Å[9]	6500	HH/HD 5 HD/DD 5 HH/DD 25	5.6	12.65	47.5	2.3	0.55	HH/HD 3.4 HD/DD 3.4

[a] Values proposed in ref. 11. [b] Natural H-bond coordinates $q_1 = \frac{1}{2}(r_{OH} - r_{HO})$, $q_2 = r_{OH} + r_{HO}$ taken from ref. 41. [c] PM3-MO calculations of *syn*/*anti* form according to ref. 32*c*.

Mechanisms of double proton transfer in amidines and related systems

General remarks. Before we discuss the kinetic parameters obtained in detail, let us make some general remarks. Firstly, we note that the Arrhenius curves of DPFA, DFFA and DBrFA are non-linear as expected for tunneling at low temperatures and for over-barrier reactions at high temperatures. Furthermore, the rate constants of the diarylamidines are very similar (Table 6), *i.e.* major effects of substituents or liquid/solid state effects are absent. This is demonstrated also in the use of a single pre-exponential factor of $10^{12.4}$ s^{-1} for all diarylamidines in the solid and liquid state. As mentioned above, this value is typical for intramolecular H transfers in the absence of pre-equilibria and major solvent reorientation during the proton transfer.[11] We note that in order to derive the intrinsic rate constants in the hydrogen bonded dimers of DPFA and DFFA dissolved in tetrahydrofuran the non-linear dependence of the pseudo-first order rate constants as a function of concentration had been analyzed.[1,2] This analysis is now confirmed by the solid state studies, especially in the case of DPFA. Here, the solid state lifts the degeneracy of the tautomerism in the liquid state. Hence, the forward rate constants k_{12}^{HH} are a little bit smaller, and the backward rate constants k_{21}^{HH} a little bit larger than their average k^{HH} found for the liquid state, as is illustrated in Fig. 12.

Finally, we note a very large variation of the rate constants in the different double proton transfers listed in Table 6. At room temperature, the transfer is fastest in the OHO hydrogen bonds of benzoic acid dimers, *i.e.* 10^{11} s^{-1}, about 10^7 s^{-1} in the amidines, 10^4 s^{-1} in 3,5-diphenyl-4-bromopyrazole DPBrP and only 10^1 s^{-1} in the oxalamidine OA7.

Kinetic HH/HD/DD isotope effects. We obtain for the amidines at high temperatures two large kinetic HH/HD and HD/DD isotope effects showing that eqn (12) is fulfilled. The same is true also for the dimers of benzoic acid (Fig. 13b)[34] and of DPBrP (Fig. 13c)[9] in the solid state. For the amidine and the pyrazole dimers we found that the rule of geometric mean is fulfilled within the margin of error, *i.e.* that the increase $\Delta\varepsilon$ of the barrier height by isotopic substitution of the first H by D is the same as of the second H by D (Table 6). In the case of benzoic acid dimer (Fig. 13b) the second effect is larger than the first. This could arise from a change of the H-bond geometries after deuteration, a phenomenon which has been observed recently for a solid exhibiting a strong OHN hydrogen bond.[35] Nevertheless, these findings are consistent with a mechanism where both protons loose zero-point energy in the transition state. This mechanism is often called "concerted", but it should be mentioned that this statement does not refer to the time domain but to the energy reaction surface. If this loss would arise from a single frequency, values of $\Delta\varepsilon$ between 2 and 3 kJ mol^{-1} would correspond to a frequency shift between 1100 and 1700 cm^{-1}. Thus, in the transition state a substantial amount of zero-point energy is still present.

By contrast, eqn (14) is fulfilled for the tautomerism of the oxalamidine OA7 (Fig. 13a) for which a stepwise tunneling process has been demonstrated.[11,26] Here, only the first substitution of H by D leads to an increase in the barrier height as only a single proton is transferred in a given reaction step. Thus, the overall kinetic HH/DD isotope effects are substantially smaller than in the diarylamidines.

A stepwise photoinduced double proton transfer has been demonstrated for 7-azaindole dimers (Fig. 13d) in condensed phases. Evidence for a photoinduced double proton transfer in 7-azaindole dimers was obtained by Kasha *et al.*[36] Femtosecond studies of Zewail *et al.*[37] indicate two reactions steps as illustrated in Fig. 13d, which was confirmed by high-level *ab initio* calculations.[38] The second step exhibited a primary

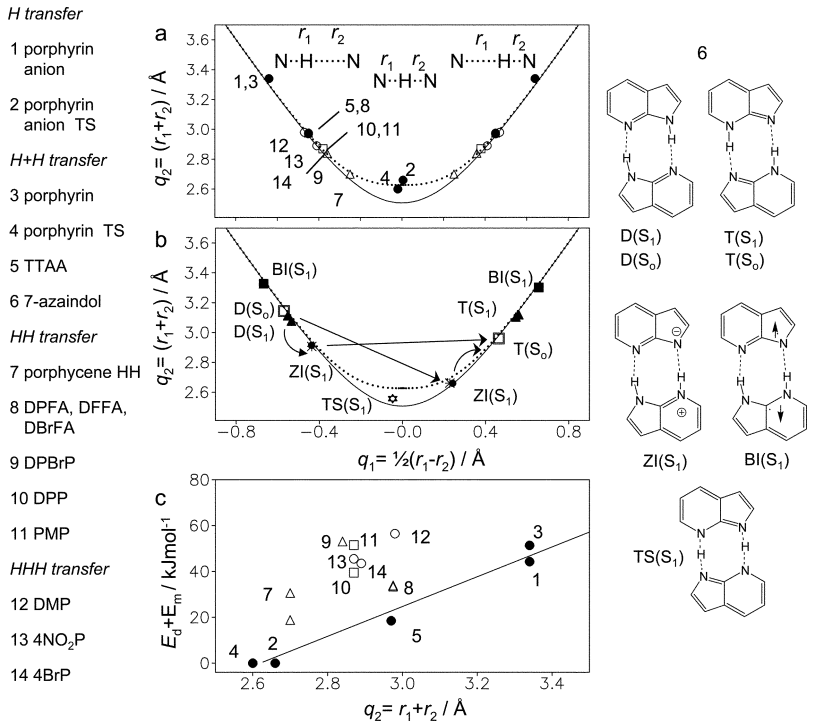

Fig. 14 (a) Hydrogen bond geometries of various molecular systems containing NHN hydrogen bonds (taken from Table 5 of ref. 11). (b) Calculated hydrogen bond geometries of various dimers of 7-azaindole in the ground state S_0 and the first excited electronic state S_1 according to ref. 38. (c) Barrier heights of the H transfers calculated from the Arrhenius curves of the species in (a). The barrier heights of the transition states are set to zero (taken from Table 5 of ref. 11). Abbreviations: TTAA: tetramethyldibenzotetraaza[14]annulene, DPBrP: 3,5-diphenyl-4-Br-pyrazole dimers, DPP: 3,5-diphenyl-pyrazole tetramers, PMP: 3-phenyl-5-methyl-pyrazole tetramers, DMP: 3,5-dimethyl-pyrazole trimers, $4NO_2P$: 4-nitropyrazole trimers, 4BrP: 4-bromo-pyrazole trimers.

kinetic H/D isotope effect of 4.7 and a secondary effect of 1.9, which were related to rates of barrier crossing and tunneling.[37b,c] We note that these values are of the same order as found here for the amidines in spite of the difference of the reaction time scales.

Barrier width and heavy atom tunneling

As mentioned above, in order to describe the low-temperature part of the HH Arrhenius curve one needs to adjust the barrier width $2a^{HH}$ which was of the order of 0.5 Å. The temperature-independent kinetic isotope effect in this regime is then determined by the contribution of heavy atom displacements to the tunneling mass, Δm, besides the values of $\Delta\varepsilon$ which was, however, already fixed in order to reproduce the kinetic isotope effects at high temperatures. We needed values of Δm between 0.5 a.m.u. for the diarylamidines and 2.3 a.m.u. for the pyrazoles. This result is surprising, but could arise both from single–double bond interconversions during the proton tunneling process and from small angle molecular flips.

For the barrier widths we needed values between 0.4 and 0.5 Å in order to reproduce the kinetic data of the amidines. Surprisingly, similar values were found before for benzoic acid dimers (Table 6). The O···O distance of benzoic acid dimers is 2.606 Å, and neutron structural data indicate a distance of 0.62 Å between the two proton sites of the OHO hydrogen bonds. If one substracts the contribution of the ground state vibrational wave function which is of the order of 0.1–0.2 Å we find a good agreement with the barrier width derived from the Arrhenius curves. Why then is the barrier width for the amidines not larger, in view of the large N···N distance of 2.963 Å, from which one can estimate that the proton sites are separated by at least 0.7 Å?

Minimum energy for tunneling to occur and barrier height. In order to answer this question let us consider the minimum energy E_m for tunneling occur. The latter is very small in the case of benzoic acid dimers, where it is dominantly arising from the energy difference between the two tautomeric states induced by the crystal fields.[35] Hence, the molecular reorganization energy in order to reach the tunneling configuration is also small. In other words, no hydrogen bond compression is needed in order to reach the tunneling configuration. Thus, there is no large difference between the barrier width and separation of the proton sites in the OHO hydrogen bond. This is consistent with the small O···O distance of 2.606 Å which is not far away from the minimum distance of OHO hydrogen bonds of about 2.4 Å.[11] The small value of the barrier width in the amidines is then understandable in the presence of substantial hydrogen bond compression, which requires a substantial amount of energy contributing to E_m. In the case of DBrFA, the value of 9.2 kJ mol^{-1} (Table 6) could be determined without assumptions from the slope of the Arrhenius curve of the HH reaction at low temperatures. As the crystal structure of DBrFA represents the best possible configuration for the tautomerism, it is plausible that the values of E_m for DPFA and DFFA are somewhat larger than

the value of DBrFA. Using this condition, we derived a value of 11.7 kJ mol^{-1} from the simulation of the Arrhenius curves of DPFA and DFFA. This value is larger than anticipated previously,[2,11] where the data of DBrFA *i.e.* the condition $E_m > 9.2$ kJ mol^{-1} were not yet available. We associate the difference, *i.e.* 2.5 kJ mol^{-1}, to the reorientation of the aryl groups in tetrahydrofuran as discussed in the next section.

Hydrogen bond compression and aryl group reorientation. Hydrogen bond compression as a major phenomenon in the tautomerism of amidines has been discussed previously.[2b] However, only in recent years hydrogen bond correlations have been established by which the compression can be quantified. Fig. 14a depicts the correlated NHN hydrogen bond coordinates of various systems in their initial stationary states containing NHN hydrogen bonds, taken from ref. 11. In the case of porphyrin[39] and its anion,[40] the coordinates of the transition states calculated using *ab initio* methods have been included, otherwise the data were derived experimentally. The solid line refers to the equilibrium geometries, *i.e.* to those of the groundstates of harmonic oscillators, whereas the dotted line includes a correction for anharmonic groundstate vibrations. We note that all geometries are located on the predicted correlation curve, especially the coordinates of the transition states of porphyrin and of its anion, exhibiting values of 2.60 and 2.66 Å. This means that hydrogen bond compression is the most important heavy atom motion which enables H-transfer; the transition state structures correspond to those expected for the strongest possible NHN hydrogen bonds, whereas the initial states do not show any sign of hydrogen bonding.

In Fig. 14b we have made a similar graph for the structures of dimers of isolated 7-azaindole in different molecular states as calculated by Serrano-Andrés and Merchán.[38] The graph of Fig. 14b demonstrates nicely the coupling of the proton coordinate q_1 to the heavy atom coordinate q_2. The initial state is the dimer in the S_1 state, $D(S_1)$. A single proton transfer occurs from the pyrrole to the pyridine ring forming the zwitterionic intermediate $ZI(S_1)$, exhibiting stronger *i.e.* shorter H-bonds as the parent dimer. Thus, this H-transfer is accompanied by a heavy atom motion or hydrogen bond compression. By contrast, the second H-transfer to the tautomer dimer $T(S_1)$ involves smaller heavy atom motions. Hence, if both process take place by tunneling, the first step will exhibit a smaller kinetic H/D isotope effect as compared to the second, because of the increase of the tunneling masses which is consistent with the experimental findings[37b,c] discussed above. A concerted transfer *via* the transition state $TS(S_1)$ involves a larger energy and could be excluded. A covalent biradical intermediate $BI(S_1)$ was proposed for the isolated dimers; its hydrogen bonds are long and weak as indicated in the graph.

The question arises whether and how the intrinsic barrier of the symmetric H transfers depends on the hydrogen bond geometries. In Fig. 14c, therefore, the experimental values of the total barrier $E_d + E_m$ are plotted as a function of q_2. As a reference, the values of zero for the transition states calculated for porphyrin and for the anion are included. As indicated by

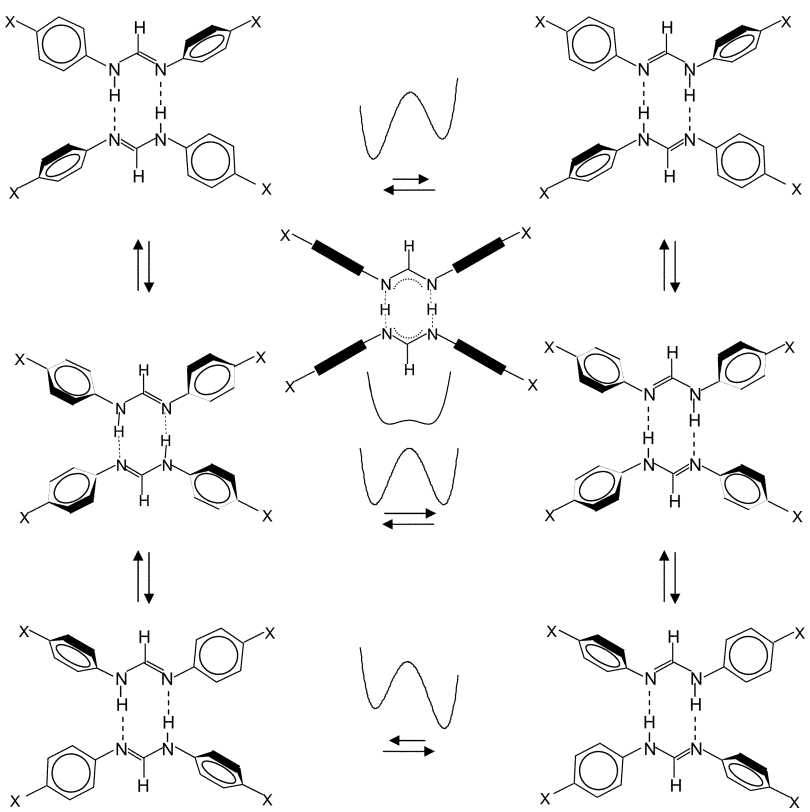

Fig. 15 Aryl group torsion, hydrogen bonding and double proton transfer in diarylformamidines. One-dimensional schematic potential curves for the double proton transfer are included.

the straight line, the total barrier of single H transfer and stepwise H + H transfer increases with increasing q_2. For the HH transfer, stepwise HH + HH transfers and HHH transfers the barriers are larger, and also increase on average with q_2 but there are deviations from the correlation. For example, porphycene exhibits shorter hydrogen bonds than the *N*,*N*-diarylformamidines, but the barrier is larger than in the latter.

This observation could arise from the balance between the reduction of the barrier by hydrogen bond compression and the energy needed for the compression. This balance can be different for the different systems, leading to transition state geometries which may not reach the maximum compression point as reached in the case of porphyrins. In other words, a system with shorter hydrogen bonds may exhibit a larger barrier as the compression energy may be larger because of a certain molecular structure.

We note that the energy needed for the compression will show up both in the minimum energy E_m for tunneling to occur and in the barrier E_d, and is, therefore, experimentally not easily obtained.

In the case of *N*,*N*-diarylformamidines, the conformation of the aryl groups influences the double proton transfer as illustrated in Fig. 15. As discussed in the Introduction, the double proton transfer is degenerate only if the torsional angles ϕ of the aryl groups (Fig. 3) are all around 30°, as is the case for DBrFA. Deviations from these angles lift the degeneracy of the transfer. It is plausible to assume that the reorientation of the aryl groups is hindered in the solid state by intermolecular interactions, leading then only to a few *N*,*N*-diarylformamidines which can react in this phase. By contrast, the aryl group reorientation energy will be much smaller in the liquid state. Therefore, we find a surprisingly excellent agreement of the rate constants of the *N*,*N*-diarylformamidines tautomerism in the liquid and the solid state.

Conclusions

The tautomerism of cyclic *N*,*N*-diarylformamidines dimers is a very good example of how molecular function is influenced by intermolecular interactions, which are controlled by intramolecular conformation and hence molecular structure as was illustrated in Fig. 1 and 2. The transfer exhibits two large HH/HD and HD/DD isotope effects and is, therefore, concerted on the energy reaction surface. Tunneling plays an important role; at low temperatures an isotope insensitive minimum energy for tunneling is required for tunneling to occur. Arrhenius curve simulations were performed using the Bell–Limbach tunneling model which does not preclude the application of more sophisticated models in the future.

Acknowledgements

We thank Prof. G. S. Denisov, St. Petersburg State University, for helpful discussions and reading this manuscript. This work was supported by the Deutsche Forschungsgemeinschaft, Bonn, and the Fonds der Chemischen Industrie, Frankfurt.

References

1 L. Meschede, D. Gerritzen and H. H. Limbach, *Ber. Bunsen-Ges. Phys. Chem.*, 1988, **92**, 469–485.
2 (*a*) H. H. Limbach, L. Meschede and G. Scherer, *Z. Naturforsch.*, 1989, **44a**, 459–471; (*b*) L. Meschede and H. H. Limbach, *J. Phys. Chem.*, 1991, **95**, 10267–10280.
3 F. Männle and H. H. Limbach, *Angew. Chem., Int. Ed. Engl.*, 1996, **35**, 441–442.
4 H. H. Limbach, F. Männle, C. Detering and G. S. Denisov, *Chem. Phys.*, 2005, **319**, 69–92.
5 R. Anulewicz, *Acta Crystallogr., Sect. C*, 1997, **C53**, 345–346.
6 R. Anulewicz, I. Wawer, T. M. Krygowski, F. Männle and H. H. Limbach, *J. Am. Chem. Soc.*, 1997, **119**, 12223–12230.
7 F. Männle, I. Wawer and H. H. Limbach, *Chem. Phys. Lett.*, 1996, **256**, 657–662.
8 (*a*) F. Aguilar-Parrilla, G. Scherer, H. H. Limbach, M. C. Foces-Foces, F. H. Cano, J. A. S. Smith, C. Toiron and J. Elguero, *J. Am. Chem. Soc.*, 1992, **114**, 9657–9659; (*b*) F. Aguilar-Parrilla, O. Klein, J. Elguero and H. H. Limbach, *Ber. Bunsen-Ges. Phys. Chem.*, 1997, **101**, 889–901; (*c*) O. Klein, M. M. Bonvehi, F. Aguilar-Parrilla, J. Elguero and H. H. Limbach, *Isr. J. Chem.*, 1999, **34**, 291–299.
9 O. Klein, F. Aguilar-Parrilla, J. M. Lopez, N. Jagerovic, J. Elguero and H. H. Limbach, *J. Am. Chem. Soc.*, 2004, **126**, 11718–11732.
10 (*a*) D. Gerritzen and H. H. Limbach, *J. Am. Chem. Soc.*, 1984, **106**, 869–879; (*b*) H. H. Limbach, O. Klein, J. M. López del Amo and J. Elguero, *Z. Phys. Chem.*, 2004, **217**, 17–49.
11 H. H. Limbach, Single and multiple hydrogen/deuterium transfer reactions in liquids and solids, in *Hydrogen Transfer Reactions*, ed. J. T. Hynes, J. Klinman, H. H. Limbach and R. L. Schowen, Wiley-VCH, Weinheim, 2007, vol. 1 & 2, ch. 6, pp. 135–221 and references cited therein.
12 H. H. Limbach, J. M. Lopez and A. Kohen, *Philos. Trans. R. Soc. London, Ser. B*, 2006, **361**, 1399–1415.
13 (*a*) P. Svensson, N. A. Bergmann and P. Ahlberg, *Z. Naturforsch.*, 1989, **44a**, 473–479; (*b*) K. A. Nguyen, M. S. Gordon and D. G. Truhlar, *J. Am. Chem. Soc.*, 1991, **113**, 1596–1600.
14 L. Claisen, *Ann. Chem.*, 1895, **287**, 366–368.
15 (*a*) T. Axenrod, P. S. Pregosin, M. J. Wieder, E. D. Becker, R. B. Bradley and G. W. A. Milne, *J. Am. Chem. Soc.*, 1971, **93**, 6536–6541; (*b*) J. Oszczapowicz, R. Orlinski and E. Hejchman, *Polish J. Chem.*, 1979, **53**, 1259–1265.
16 D. G. Ott, in *Synthesis with Stable Isotopes*, John Wiley & Sons, New York, 1981.
17 P. Du Bois Murphy, *J. Magn. Reson.*, 1986, **70**, 307–312.
18 D. Torchia, *J. Magn. Reson.*, 1978, **30**, 613–616.
19 R. D. Kendrick, S. Friedrich, B. Wehrle, H. H. Limbach and C. S. Yannoni, *J. Magn. Reson.*, 1985, **65**, 159–161.
20 H. H. Limbach, Dynamic NMR spectroscopy in the presence of kinetic hydrogen deuterium isotope effects, in *NMR Basic Principles and Progress*, Heidelberg, Berlin, 1990, vol 26, ch. 2.
21 (*a*) S. Alexander, *J. Chem. Phys.*, 1962, **37**, 974–980; (*b*) G. Binsch, *J. Am. Chem. Soc.*, 1969, **91**, 1304–1309; (*c*) D. A. Kleier and G. Binsch, *J. Magn. Reson.*, 1970, **3**, 146–160.
22 (*a*) H. H. Limbach, J. Hennig, R. D. Kendrick and C. S. Yannoni, *J. Am. Chem. Soc.*, 1984, **106**, 4059–4060; (*b*) B. Wehrle, H. Zimmermann and H. H. Limbach, *J. Am. Chem. Soc.*, 1988, **110**, 7014–7024; (*c*) H. H. Limbach, B. Wehrle, M. Schlabach, R. D. Kendrick and C. S. Yannoni, *J. Magn. Reson.*, 1988, **77**, 84–100; (*d*) B. Wehrle and H. H. Limbach, *Chem. Phys.*, 1989, **136**, 223–247.
23 (*a*) F. Aguilar-Parrilla, B. Wehrle, H. Bräunling and H. H. Limbach, *J. Magn. Reson.*, 1990, **87**, 592–597; (*b*) B. Wehrle, F. Aguilar-Parrilla and H. H. Limbach, *J. Magn. Reson.*, 1990, **87**, 584–591.
24 C. G. Hoelger, B. Wehrle, H. Benedict and H. H. Limbach, *J. Phys. Chem.*, 1994, **98**, 843–851.
25 W. Medycki, E. C. Reynhardt and L. Latanowicz, *Mol. Phys.*, 1998, **93**, 323–327.
26 G. Scherer and H. H. Limbach, *J. Am. Chem. Soc.*, 1994, **116**, 1230–1239.
27 J. Braun, M. Schlabach, B. Wehrle, M. Köcher, E. Vogel and H. H. Limbach, *J. Am. Chem. Soc.*, 1994, **116**, 6593–6604.

28 J. Basran, L. Masgrau, M. J. Sutcliffe and N. Scrutton, Solution and computational studies of kinetic isotope effects in flavoprotein and quinoprotein catalyzed substrate oxidations as probes of enzymic hydrogen tunneling and mechanism, in *Isotope Effects in Chemistry and Biology*, ed. A. Kohen and H. H. Limbach, Taylor & Francis, Boca Raton FL, 2006, ch. 25, pp. 671–690.
29 M. J. Knapp, M. Meyer and J. P. Klinman, Nuclear tunneling in the condensed phase: hydrogen transfer in enzyme reactions, in *Hydrogen Transfer Reactions*, ed. J. T. Hynes, J. Klinman, H. H. Limbach and R. L. Schowen, Wiley-VCH, Weinheim, 2007, vol. 3 & 4, ch. 10, pp. 1241–1284 and references cited therein.
30 R. A. Marcus, *Faraday Discuss. Chem. Soc.*, 1982, **74**, 7–15.
31 A. Fernández-Ramos, Z. Smedarchina and J. Rodríguez-Otero, *J. Chem. Phys.*, 2001, **114**, 1567–1574.
32 (*a*) G. Scherer and H. H. Limbach, *J. Am. Chem. Soc.*, 1989, **111**, 5946–5947; (*b*) G. Scherer and H. H. Limbach, *J. Am. Chem. Soc.*, 1994, **116**, 1230–1239; (*c*) G. Scherer and H. H. Limbach, *Croat. Chim. Acta*, 1994, **67**, 431–440.
33 (*a*) B. H. Meier, F. Graf and R. R. Ernst, *J. Chem. Phys.*, 1982, **76**, 767–774; (*b*) A. Stöckli, B. H. Meier, R. Kreis, R. Meyer and R. R. Ernst, *J. Chem. Phys.*, 1990, **93**, 1502–1520; (*c*) A. Heuer and U. Haeberlen, *J. Chem. Phys.*, 1991, **95**, 4201–4124; (*d*) J. L. Skinner and H. P. Trommsdorff, *J. Phys. Chem.*, 1988, **89**, 897–907; (*e*) R. Meyer and R. R. Ernst, *J. Chem. Phys.*, 1990, **93**, 5518–5532; (*f*) Y. Kim, *J. Am. Chem. Soc.*, 1996, **118**, 1522–1528; (*g*) Y. Kim, *J. Phys. Chem. A*, 1998, **102**, 3025–3036.
34 Q. A. Xue, A. J. Horsewill, M. R. Johnson and H. P. Trommsdorff, *J. Chem. Phys.*, 2004, **120**, 11107–11119.
35 J. Zhou, Y. S. Kye and G. S. Harbison, *J. Am. Chem. Soc.*, 2004, **126**, 8392–8393.
36 C. A. Taylor, M. A. El-Bayoumi and M. Kasha, *Proc. Natl. Acad. Sci. U. S. A.*, 1969, **63**, 253–260.
37 (*a*) A. Douhal, S. K. Kim and A. H. Zewail, *Nature*, 1995, **378**, 260–263; (*b*) T. Fiebig, M. Chachisvilis, M. Manger, A. H. Zewail, A. Douhal, I. Garcia-Ochoa and A. de La Hoz Ayuso, *J. Phys. Chem. A*, 1999, **103**, 7419–7431; (*c*) O. H. Kwon and A. H. Zewail, *Proc. Natl. Acad. Sci. U. S. A.*, 2007, **104**, 8703–8708.
38 L. Serrano-Andrés and M. Merchán, *Chem. Phys. Lett.*, 2006, **418**, 569–575.
39 D. K. Maity, R. L. Bell and T. N. Truong, *J. Am. Chem. Soc.*, 2000, **122**, 897–906.
40 T. Vangberg and A. Ghosh, *J. Phys. Chem. B*, 1997, **101**, 1496–1497.
41 T. Emmler, S. Gieschler, H. H. Limbach and G. Buntkowsky, *J. Mol. Struct.*, 2004, **700**, 29–38.